Environmental Pollution 401 (2026) 128232

Contents lists available at ScienceDirect

Environmental Pollution

journal homepage: www.elsevier.com/locate/envpol

$PM_{2.5}$ composition at an atmospheric ammonia hotspot in Europe

Miguel Escudero [a,*], Natividad Miguel [b], José Hernández de la Torre [c], Miguel Arner [c], Julia Marín-Sáez [d], Juan Hierro [e], Andrés Alastuey [f], Xavier Querol [f], Cristina Reche [f], Amalia Muñoz [g], Esther Borrás [g], Jorge Pey [h]

[a] Department of Applied Physics, Universidad de Zaragoza, Escuela de Ingeniería y Arquitectura, María de Luna 3, Zaragoza, 50018, Spain
[b] Water and Environmental Health Research Group, University Institute for Research in Environmental Sciences of Aragón, Department of Chemical Engineering and Environmental Technologies, University of Zaragoza, Escuela Politécnica Superior, Ctra. de Cuarte s/n, Huesca, 22071, Spain
[c] Universidad de Zaragoza, Escuela Politécnica Superior, Ctra. de Cuarte s/n, Huesca, 22071, Spain
[d] Department of Applied Physics, Universidad de Zaragoza, Escuela Politécnica Superior, Ctra. de Cuarte s/n, Huesca, 22071, Spain
[e] Centro Universitario de la Defensa, Academia General Militar, Ctra. de Huesca s/n, Zaragoza, 50090, Spain
[f] Institute of Environmental Assessment and Water Research (IDAEA-CSIC), Jordi Girona 18-26, Barcelona, 08034, Spain
[g] Fundación Centro de Estudios Ambientales del Mediterráneo (CEAM), Associate Unit CSIC-CEAM "Atmospheric Pollution", Parque Tecnológico, Charles Darwin 14, Paterna (Valencia), 46980, Spain
[h] Instituto Pirenaico de Ecología (IPE), CSIC, Av. Montañana 1005, Zaragoza, 50059, Spain

ARTICLE INFO

Keywords:
Agricultural emissions
Secondary inorganic aerosols
Spain
Ebro valley
Source contribution

ABSTRACT

Fine particulate matter ($PM_{2.5}$) pollution poses a significant environmental risk to human health, ecosystems, and climate, both across Europe and globally. Ammonia (NH_3), primarily emitted by agro-livestock activities, is a major precursor gas for secondary particulate formation; critically, however, it remains largely unregulated in European directives and is seldom monitored within conventional air quality networks. This study investigates the chemical composition, formation mechanisms, and potential sources of $PM_{2.5}$ within a critical European agricultural region (Central Ebro Valley, CEV), recognized as a major atmospheric NH_3 hotspot. NH_3 concentration and $PM_{2.5}$ chemical composition data were collected during two intensive campaigns spanning distinct winter and summer seasonal regimes. Results demonstrate that the study area is characterized by an NH_3-saturated environment, which fundamentally controls $PM_{2.5}$ formation dynamics and leads to severe regional pollution episodes. The high ammoniacal availability is identified as a key factor promoting the generation of high concentrations of Secondary Inorganic Aerosols (SIA), particularly during winter. Furthermore, the characteristic summer atmospheric dynamics, featuring high vertical dispersion driven by the intense development of the Planetary Boundary Layer (PBL), enhances the region's role as an atmospheric NH_3 reservoir for the wider Mediterranean Basin, establishing it as a major source area in Southern Europe. A preliminary source contribution analysis based on Positive Matrix Factorization (PMF) identified five factors with marked seasonality, confirming the unquestionable impact of agro-livestock NH_3 emissions, biomass burning, mineral resuspension from arid land surfaces, and African dust intrusion during summer. This study underscores the critical importance of policy decisions targeting emission controls within the agricultural and livestock sectors to effectively mitigate $PM_{2.5}$ levels locally and regionally.

1. Introduction

Despite declining pollutant levels, air pollution remains a critical environmental risk in Europe. The European Environmental Agency reported 239,000 premature deaths in 2022 due to chronic $PM_{2.5}$ exposure. $PM_{2.5}$ is linked to respiratory (asthma, COPD, lung cancer) and cardiovascular diseases (strokes, heart failure), alongside neurological disorders and diabetes (WHO, 2021; Best Rogowski et al., 2025). Furthermore, PM causes ecosystem eutrophication and acidification (Rai, 2016), alters Earth's energy balance (IPCC, 2023), and deteriorates materials (Al-Thani et al., 2018).

PM is a complex mixture of solid and liquid aerosols. Secondary inorganic aerosols (SIA), primarily ammonium sulphate ($(NH_4)_2SO_4$) and ammonium nitrate (NH_4NO_3), constitute a large part of $PM_{2.5}$. These form via gas-to-particle processes involving SO_2, NO_2, and NH_3 (Behera and Sharma, 2012). However, European emission reductions for these precursors have been uneven (EEA, 2025). Since 2005, SO_x and NO_x

* Corresponding author.
E-mail address: mescu@unizar.es (M. Escudero).

https://doi.org/10.1016/j.envpol.2026.128232
Received 11 February 2026; Received in revised form 9 April 2026; Accepted 28 April 2026
Available online 8 May 2026

emissions fell by 84% and 53% respectively, while NH_3 decreased by only 17%. As primary $PM_{2.5}$ emissions also fell by 37%, secondary species are increasingly dominant in European fine PM (Chen et al., 2022).

NH_3 is the atmosphere's primary alkaline gas. Its most significant health impact is the formation of fine PM (WHO, 2021, 2025). While gaseous ammonia causes acute issues at concentrations typically found in industrial or agricultural settings (Wing and Wolf, 2000; Naseem and King, 2018), long-term exposure to lower concentrations also poses risks (Wyer et al., 2022). NH_3 also contributes significantly to nitrogen pollution, driving acidification and eutrophication in terrestrial and aquatic ecosystems (Fowler et al., 2015).

Approximately 93% of European NH_3 originates from agriculture and livestock (Sutton et al., 2008). In urban areas, other sources become significant; for instance, selective catalytic reduction (SCR) technology in new diesel vehicles generates substantial traffic emissions of ammonia (Hopke and Querol, 2022). Additionally, urban NH_3 levels correlate with garbage container density (Reche et al., 2012). Satellite data and modeling reveal three European NH_3 hotspots (Clarisse et al., 2009; Van Damme et al., 2014; Dammers et al., 2019; Tichý et al., 2023): Central Europe (fertilization and livestock), the Po Valley (industrial/traffic emissions and stagnant conditions), and the central Ebro Valley (intensive farming).

NH_3 surface measurements face comparability challenges due to methodological variety. Twigg et al. (2022) demonstrated that while 13 instruments performed accurately at high concentrations, consistency declined below 10 ppb. Notably, chemiluminescence-based devices used in some European networks have yielded poorer results in intercomparison studies (Schwab et al., 2007). However, a general pattern is that NH_3 levels remain highly dependent on local agricultural proximity; Liu et al. (2024) found concentrations in intense agricultural areas (14.1 ± 10.8 μg m^{-3}) four times higher than in non-agricultural regions (3.2 ± 1.8 μg m^{-3}).

Inventories show a modest 17% reduction in NH_3 emissions between 2005 and 2023 (EEA, 2025), the smallest decrease among pollutants regulated by the National Emission reduction Commitments Directive. While (Tichý et al., 2023) estimated declines in central and western Europe (37%–38%), Southern Europe saw a much smaller reduction (7.6%). However, these inventory trends often conflict with experimental observations. Van Damme et al. (2021) observed NH_3 column concentrations increasing in western and southern Europe at $1.90 \pm 0.43\%$ yr^{-1} (2.08% in Spain) between 2008 and 2018. Surface data similarly shows increases in Barcelona (+9.4%) and mountain sites (+16%) (Reche et al., 2022). Liu et al. (2024) reported significant increases at regional background stations in agricultural areas that could be attributed to an actual emission increase or due to reduced NH_3 consumption for secondary aerosols responding to lower SO_2 and NO_x availability.

Despite policy-driven PM reductions in Europe and Spain (Querol et al., 2014; in't Veld et al., 2021), $PM_{2.5}$ toxicity is an escalating concern due to shifting chemical compositions. Specific components, such as metals (V, Ni) and carbonaceous aerosols, exert greater health impacts than other constituents (Kelly and Fussell, 2012; Bell et al., 2014; Hime et al., 2018; Park et al., 2018). Secondary organic aerosols (SOA), known for their potent oxidative capacity, contribute significantly to this toxicity (Jiang et al., 2016; Daellenbach et al., 2020).

In Spain, the rising contribution of secondary organic aerosols (SOA) to particulate matter is driven by three primary factors. First, a shift in the photochemical environment characterized by rising ozone levels and declining SO_2 and NO_x has created an atmosphere rich in hydroxyl and nitrate radicals that accelerates SOA formation (Saiz-Lopez et al., 2017). Second, the proliferation of SUV-type vehicles has led to an increase in volatile organic compound (VOC) emissions (Frey, 2018). Finally, biomass burning from both domestic heating and agricultural waste remains a significant source; these emissions are capable of long-distance dispersion and notably impact regional fine PM mass (Reche et al., 2012; Viana et al., 2013; Amato et al., 2016; Domínguez et al., 2025).

This study characterizes $PM_{2.5}$ and NH_3 in the central Ebro Valley, a European paradigm for intense agricultural and livestock emissions. These sources, alongside biomass combustion (domestic and agricultural), generate significant NH_3 and carbonaceous products. Unlike previous Spanish studies focused on urban areas (Reche et al., 2012, 2015, 2022; Liu et al., 2024), we present results from parallel summer and winter campaigns. This research explores the relationship between NH_3 emissions and $PM_{2.5}$ formation, analyzing chemical processes and spatial–temporal variations. These findings will help identify research gaps and inform air quality management under the new European Directive, which emphasizes NH_3 as a critical $PM_{2.5}$ precursor.

2. Methodology and data

Data were obtained during two campaigns with distinct climatic conditions: summer (7–22 July 2022) and winter (23 February–10 March 2023).

2.1. Study area

The central Ebro Valley (CEV) occupies much of the Ebro River watershed, bounded by the Pyrenees to the north and the Iberian Range to the south. The landscape features limestone plateaus exceeding 600 m above sea level, carved by the Ebro and tributaries like the Cinca and Gállego (Peña and Lozano, 2004).

The CEV's cold steppe climate (Beck et al., 2018) is characterized by extreme temperatures and low precipitation (~315 mm/year), concentrated in spring and autumn. Winters are cold (with average minimum temperatures near 0°C) with frequent thermal inversions and dense fog; summers often exceed 35°C. Wind patterns are channeled along the valley axis, dominated by the cold, dry "cierzo" (W-NW) and the warmer, lighter "bochorno" (E-SE) (Cuadrat, 2004).

Zaragoza (>720,000 inhabitants in 2025) is the primary urban center and a major logistics hub, contributing significant traffic-related emissions (Escudero et al., 2014). Smaller centers include Huesca and Utebo (54,136 and 19,000 inhabitant, respectively). High-traffic motorways that cross the valley and seven thermal power plants further impact air quality. Additionally, the CEV supports an intensive agricultural and livestock sector, notably pig farming, due to favorable climate and land availability.

2.2. Determination of NH_3 concentrations

Ammonia concentrations were assessed using ALPHA-type passive samplers (Tang et al., 2001). These consist of a polypropylene cylinder sealed at one end containing a glass fiber filter impregnated with citric acid, methanol, and glycerin. A 1.2 μm Teflon filter and stainless steel mesh cover the opposite side of the cylinder facilitate molecular diffusion through a 20 mm opening.

Samplers were deployed at 4 m height on PVC supports. Duplicate measurements were taken at each point to minimize data loss, with the final NH_3 value representing the average. Despite isolated sample losses, data were retrieved for 93.6% of locations.

Filters were analyzed using the indophenol method, where chemisorbed NH_3 is converted to ammonium (NH_4^+) and determined spectrophotometrically at 653 nm. Ambient concentrations were calculated using Fick's law:

$$C = \frac{X}{TD} \cdot 0.40657$$

where C is air concentration (moles cm^{-3}), X is collected mass (moles), T is time (seconds), and D is the diffusion coefficient (0.242 for NH_3). The constant 0.40657 is derived from sampler geometry. Results were converted to μg m^{-3}.

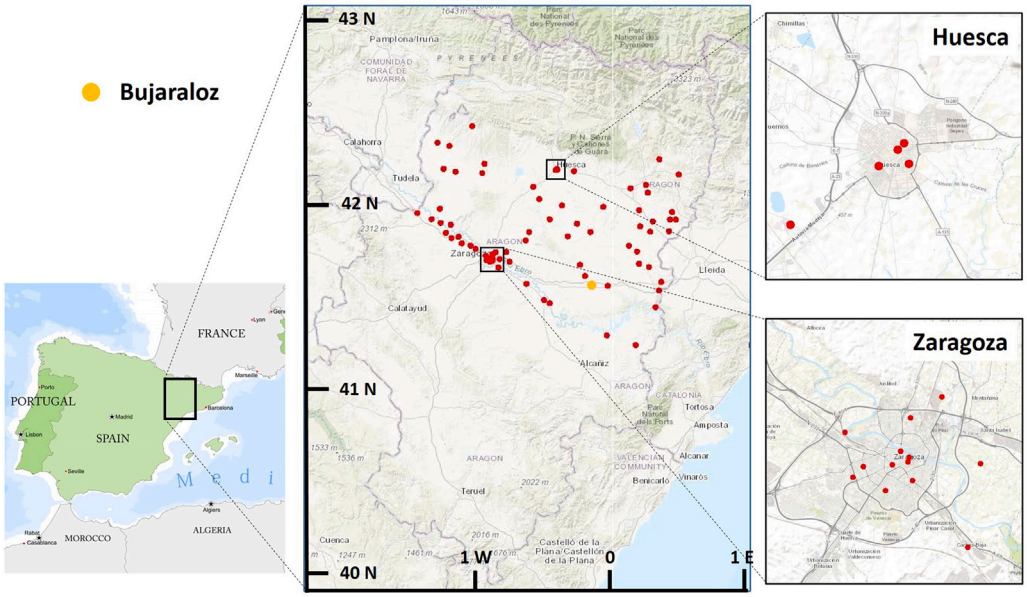

Fig. 1. Location of sampling points (n = 78) for NH_3. Highlighted in orange Bujaraloz where $PM_{2.5}$ samples where also collected. (For interpretation of the references to color in this figure legend, the reader is referred to the web version of this article.)

Passive samplers were exposed for 15 days at 78 points during each campaign. Samples were refrigerated during transport, and blanks were used to monitor contamination. Sampling points (Fig. 1 and Table S1) targeted potential NH_3 sources, prioritizing population exposure. Locations included high-density farming regions (placed in towns > 600 inhabitants), urban traffic, background and sub-urban sites in Zaragoza and Huesca, and specific sources like wastewater plants, a city market, and a logistics platform (Mercazaragoza).

2.3. $PM_{2.5}$ analyses

Daily $PM_{2.5}$ samples were collected at the Bujaraloz air quality station (Fig. 1) using a high-volume gravimetric sampler (30 m^3 h^{-1}) on PALLFLEX quartz fiber filters following EN 12341 procedure. Fifteen filters per campaign were collected, coinciding with NH_3 monitoring.

Following gravimetric mass determination, filters were chemically analyzed. A quarter of each filter was placed in a 60 ml PFA bomb (75 psi) along with 2.5 ml HNO_3 and 5 ml HF. The bombs were sealed and placed in an oven at 90°C, then evaporated on a plate at 250°C. Once a dry residue was obtained, it was dissolved by adding 2.5 ml of HNO_3, bi-distilled water (MilliQ grade) was added, and the solution was made up to 25 ml in a volumetric flask to obtain final 5% HNO_3 solutions, which were subsequently analyzed. The concentrations of the elements of interest in the resulting solutions from the acid digestion of the filters were analyzed by Inductively Coupled Plasma Atomic Emission Spectrometry (ICP-AES) for major elements and by Inductively Coupled Plasma Mass Spectrometry (ICP-MS) for trace elements. For every batch of 30 filters, an equivalent fraction of 2 blank filters was digested. The concentrations obtained from the blank filters were subtracted from the concentrations determined in the sampled filters.

For the determinations of soluble phases (NH_4^+, Cl^-, SO_4^{2-}, and NO_3^-), a quarter of the filter was leached with 30 ml of MilliQ bi-distilled water at 60°C in sealed PFA bombs for 12 h. Once the leachates were obtained, they were centrifuged and the resulting solutions (25 ml) were analyzed. The concentrations of Cl^-, SO_4^{2-}, and NO_3^- were measured with an ion chromatograph (IC, Dionex Aquion Thermo Scientific). NH_4^+ concentrations were measured with a selective electrode (Thermo Scientific model Orion 9512HPBNWP).

The determination of elemental and organic carbon concentrations (EC and OC) was performed with a SUNSET thermo-optical analyzer using the UNE-EN 16909 procedure to measure EC and OC in ambient particulate matter samples deposited on filters. The method is based on the volatilization and oxidation of carbon-containing PM components, quantification of the released carbon, and optical correction for pyrolytic carbon (PC). Therefore, a filter punch (1 cm^2) was placed in the instrument's oven and purged with helium. In the first mode (inert carrier gas), the oven temperature was increased to volatilize OC. The carrier gas was then switched to 2% O_2 in He and a second temperature ramp was initiated.

The concentration of SiO_2 is estimated from the concentration of Al_2O_3 ($SiO_2 = 3Al_2O_3$). The concentration of OM is obtained from that of OC using the ratio OM = 1.7·OC for winter and OM = 2.0·OC for summer, taking typical values from Font et al. (2024) and assuming that in summer the aerosol in this area is considerably oxidized and aged.

2.4. NH_3 emissions estimation

A model was developed to estimate total ammoniacal nitrogen (TAN) emissions from livestock within a 5 km radius of each sampling point. TAN represents nitrogen released as ammonia during grazing, housing, storage, and fertilization (MITECO, 2025). The highest TAN emission percentages are observed in laying hens, turkeys, and other poultry species, reaching 80%. Cattle, goats, and broiler chickens follow with 70%. Sheep and rabbits contribute 60% of TAN emissions. For pigs, adult swine account for 72.9% of TAN, while finishing pigs are at 72.8%. Regarding equine livestock, horses have a TAN emission of 70%, while other equids (donkeys and mules) have 40%.

Initially, data on the number of head of active livestock farms located within a 5 km radius of each NH_3 measurement point were obtained from the Aragonese Institute of Environmental Management (INAGA) database (INAGA, 2022). In the CEV, livestock farms are often grouped around small municipalities, so a 5 km buffer typically includes several farms of different sizes rather than a single point source. This spatial pattern supports the use of a relatively wide buffer to characterize the local emission context. As the INAGA database does not categorize livestock by specific types, the zootechnical classification of each farm was aligned with the distributions outlined in the Order of February 13, 2015 (Government of Aragón, 2015), using the definitions established in current Aragonese legislation. This Order specifies

nitrogen excretion factors based on the average Livestock Units (LU) of the main livestock species per family, in kg year^{-1} animal^{-1}.

LU is a standardized unit that allows for the comparison of different livestock categories based on animal type, age, or size. For reference, one LU is equivalent to a bull or a cow over two years old, with conversion factors established for other ages and livestock species according to Spanish legislation (see Table S2 where also nitrogen excretion factors are provided in units of kg N animal^{-1} year). In cases where a clear equivalence between the livestock categories in the Order of February 13, 2015 and those in the INAGA database could not be found, estimations were made based on livestock censuses from Aragón or, if that information was unavailable, from Spain (https://www.mapa.gob.es/es/estadistica/temas/estadisticas-agrarias/ganaderia/encuestas-ganaderas/REFS). Technical details of these estimations are presented in the supplementary information.

2.5. Exploration of $PM_{2.5}$ sources by positive matrix factorization

Positive Matrix Factorization (PMF 5.0, U.S. EPA) was used to identify and quantify potential sources contributing to the measured variables (Paatero and Tapper, 1994). In our case, we have followed the good practices recommended in the European Guide on Air Pollution Source Apportionment with Receptor Models (Belis et al., 2014). The dataset consisted of 30 samples, 15 from the summer and 15 from the winter campaign, respectively, and 30 variables. Given the limited dataset (30 samples), this work is intended as an exploratory evaluation of potential sources rather than a statistically robust apportionment analysis. Amongst the selected variables, K, Li, Cu, Se, Cd and Sn were considered as weak species. Several model runs were performed, testing different numbers of factors (from 4 to 7) in order to evaluate model stability and interpretability. The optimal solution was obtained with five factors, based on the examination of Q values (Qtrue and Qexpected), residual distributions, and the physical interpretability of factor profiles. The selected solution uses FPEAK = [0.0], which offered the most interpretable profiles without inflating model error. The final model showed Q = [Q] and Qexpected = [Qexp], giving Q/Qexpected = 1.026, which is close to 1 and indicates an acceptable fit. Model diagnostics, including scaled residuals and bootstrap uncertainty analysis, confirmed the robustness of the five-factor solution.

Uncertainties were estimated following the approach proposed by Amato et al. (2016), combining analytical uncertainties with a percentage of the measured concentrations to account for instrumental and methodological variability. In addition, a 5% extra uncertainty was added to all variables to better reflect potential measurement and sampling biases. These uncertainty estimates were used to weight the data matrix, and variables with low signal-to-noise ratios were downweighted accordingly. Despite the limited size of the dataset, model diagnostics, including the analysis of scaled residuals, bootstrap and displacement tests, confirmed the robustness and stability of the five-factor solution.

3. Results and discussion

3.1. Meteorological context of the campaigns

Meteorological data for both campaigns were extracted from four Regional Air Quality Network stations (Fuentes de Ebro, Huesca, Bujaraloz, and Monzón) within the study domain. Detailed data and plots are provided in Table S1 and Figures S1 and S2 (Supplementary Information).

3.1.1. Summer campaign

The 2022 summer campaign was exceptionally hot and dry, with negligible precipitation. Average temperatures were approximately 30°C, frequently exceeding 40°C. Average relative humidity (RH) was moderate (26%–47%), though significant diurnal dispersion occurred, with RH peaks in Bujaraloz and Monzón during the early morning hours. Wind speeds were generally light, though the Ebro Valley's (EV) channeling effect produced higher velocities at Fuentes de Ebro. Within the EV (Bujaraloz and Fuentes de Ebro), wind roses show dominant NW (stronger) and SE (lighter) components aligned with the valley axis (Figure S2). Outside the EV (Monzón and Huesca), southern winds prevailed. Temporally, temperatures peaked between 13/7 and 17/7, coinciding with minimal wind intensity and the lowest RH values. Wind was strongest from 7/7 to 10/7, primarily from the W, followed by a period of low speeds with variable directions until a slight increase in S/SE winds after 17/7.

3.1.2. Winter campaign

In contrast, the winter campaign was characterized by moderate precipitation in the eastern domain during the first sampling days. Temperatures were seasonally typical (averaging 8°C with minimums below 0°C), while RH was moderate to high (50%–57%). Average wind speeds were moderate, with the highest intensities recorded in the EV. Wind roses (Figure S2) again differentiate between EV sites (Fuentes de Ebro and Bujaraloz), which showed consistent NW/W components, and non-EV sites, which exhibited bimodal patterns: NW in Monzón and NE/SE in Huesca. During the winter campaign, temperatures decreased until reaching a minimum on March 2nd, followed by an unseasonably warm period exceeding 20°C by March 8th. RH peaked during initial rainfall events before stabilizing. Efficient channeling through the EV maintained a steady NW/W flow, whereas Monzón and Huesca showed greater variability, including daily shifts between SE and NW-W components during light-wind periods.

3.2. NH_3 concentrations

Fig. 2 show maps with ammonia concentrations obtained during the two campaigns. Exact NH_3 concentration values at each point can be found in the supplementary information (Table S1). Fig. 2 displays NH_3 maps for both campaigns; exact values are provided in Table S1. Concentrations ranged from 3.5 to 19.8 μg m^{-3} in summer (avg. 8.8 μg m^{-3}) and 2.6 to 25.4 μg m^{-3} in winter (avg. 9.3 μg m^{-3}). These levels are significant both for their magnitude and the vast geographical area affected. Highest concentrations occurred in the eastern domain and isolated western points, coinciding with high livestock density and proximity to intensive pig farming regions in Catalonia. Conversely, Ebro Valley concentrations were lower due to fewer farms and higher wind speeds, which enhanced ventilation and dilution.

Liu et al. (2024) established a European benchmark across 69 datasets, reporting a mean NH_3 concentration of 8.0 ± 8.9 μg m^{-3}. The current campaign's seasonal means (8.8 μg m^{-3} in summer and 9.3 μg m^{-3} in winter) align with this European average, while peak observations (up to ~25 μg m^{-3}) far exceed typical background levels of ~1 μg m^{-3} and instead match agricultural hotspot conditions (Liu et al., 2024). On a broader scale, global syntheses and satellite data (Liu et al., 2019) confirm that while regions like the North China Plain and northern India exceed 6 μg m^{-3}, western Europe typically falls within the 2–6 μg m^{-3} range. Furthermore, literature reviews (Nair and Yu, 2020) indicate that while the Ebro Valley's maxima are comparable to other European hotspots, they remain below the extreme monthly means of the US Midwest (14 μg m^{-3}) and the North China Plain (52 μg m^{-3}), ultimately characterizing the Ebro Valley as a prominent NH_3 hotspot within both Spanish and European contexts.

NH_3 levels were comparable across seasons but slightly higher in winter, an unusual finding for rural areas where summer peaks are typically expected due to temperature-enhanced volatilization. Two

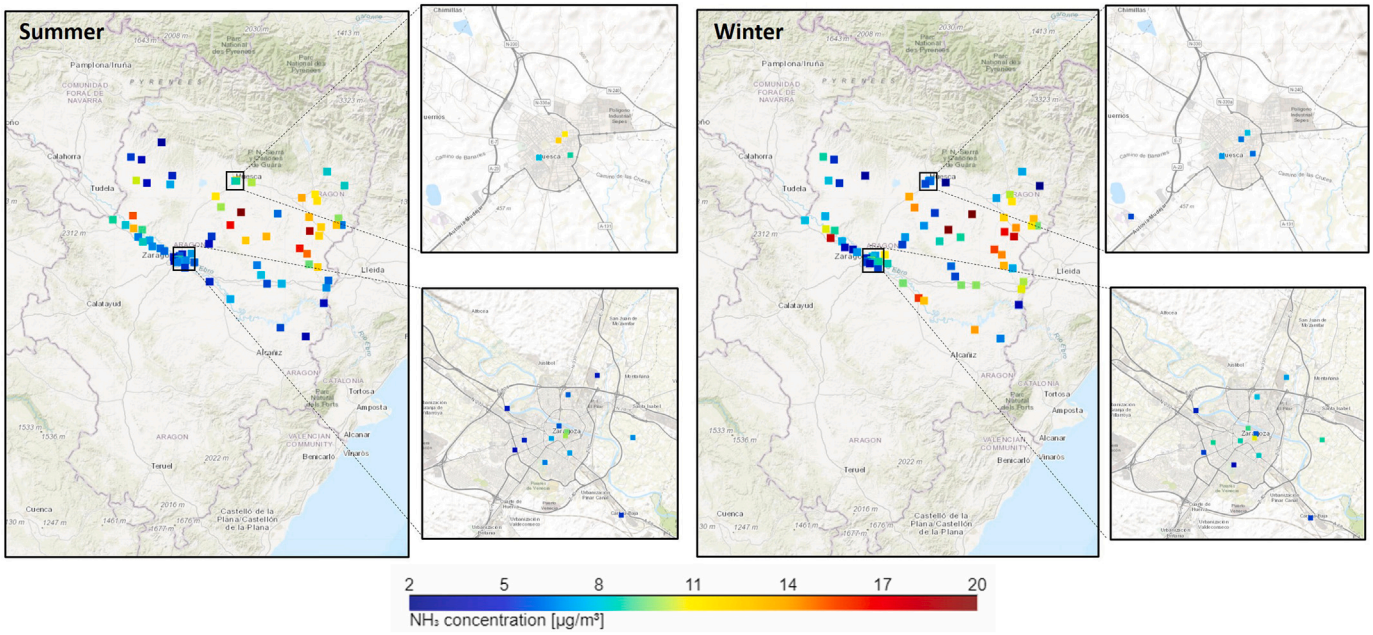

Fig. 2. NH_3 concentrations registered during the summer (7–22 July 2022) and winter (23 February–10 March 2023) campaigns in the central Ebro Valley.

factors explain this. First, high summer PBL development and thermal movements displace NH_3 upward, reducing surface concentrations. This suggests the Ebro Valley acts as a conduit where NH_3 reaches the upper troposphere and is dispersed regionally, consistent with summer peaks observed at remote mountain sites (Reche et al., 2022). Second, frequent agricultural biomass burning in late winter likely increased concentrations during the February–March campaign. Specific spatial differences (Figure S3) reflect seasonal meteorology. Summer saw higher levels in the north due to southerly transport, while winter levels peaked in the central and eastern domain as NW circulation displaced air masses from source regions toward the southeast.

In an analysis by site typology, we observed that rural points (located in small towns with populations between 600 and 10,000 inhabitants) recorded the highest concentrations, with averages of 8.9 μg m^{-3} in summer and 9.4 μg m^{-3} in winter, although there is significant variability, with points in the eastern domain easily exceeding 20 μg m^{-3} in both periods. The high levels in rural areas are clearly associated with widespread agricultural and livestock activity around these points. These levels fall within the range of values reported for European rural areas impacted by agriculture, and are substantially greater than those documented at non-agriculturally influenced rural sites in Europe (Liu et al., 2024).

In urban areas, concentrations depend on regional agricultural impact, traffic proximity, and street morphology. Central city locations often hinder dispersion, exacerbating levels from traffic and waste containers. Urban background sites in agricultural zones reached 9.0 (summer) and 10.9 (winter) μg m^{-3}. In Zaragoza and Huesca, central traffic points recorded 9 μg m^{-3} in both seasons, while non-central sites were lower (6.6–7.2 μg m^{-3}). These urban levels exceed those of major European cities like Paris, London, or Madrid, instead aligning with cities in agricultural heartlands like Milan or Münster (Reche et al., 2015, 2022; Ehrnsperger and Klemm, 2021; Manninen et al., 2023; Liu et al., 2024).

The data unequivocally establish the CEV as a major NH_3 hotspot, confirming satellite-based observations (Van Damme et al., 2014). The spatial homogeneity of these elevated levels suggests the region acts as an extensive reservoir. Persistent NH_3 availability facilitates in-situ secondary inorganic species formation, raising regional $PM_{2.5}$ background levels and contributing to long-range transport to adjacent regions.

Table 1
TAN emissions and number of livestock in the study area by livestock type. The values in this table have been calculated considering only data from livestock farms located within 5 km of the sampling points during the campaigns.

Types of livestock	TAN		Number of livestock	
	kg $year^{-1}$	%	Total	%
Swine	17,260,938	71	3,540,519	20
Cattle	4,200,449	17	265,850	1
Poultry	1,953,056	8	11,683,328	65
Small ruminants	696,183	3	359,166	2
Equine	29,015	<1	5447	<1
Rabbits	10,128	<1	43,427	<1
Other livestock	67	<1	1,984,347	11
Total	*24,149,837*	*100*	*17,882,084*	*100*

To validate the agricultural impact, TAN emissions were modeled within 5 km of each point (Table 1). Pig farming dominates, accounting for 71% of TAN emissions despite representing only 20% of the livestock population. Cattle contribute 17% (1% of population), while poultry contribute 8% (65% of population). Small ruminants and other livestock have negligible impacts. Unlike much of the EU where cattle are the primary source (Malherbe et al., 2022), the CEV is distinctively driven by swine.

Pearson's coefficients obtained comparing between NH_3 and TAN emissions within 5 km of each point demonstrate the agricultural impact on ambient levels (Figure S4). Correlation was stronger in summer ($r = 0.67$) than winter ($r = 0.39$). In rural/suburban areas, the summer correlation reached 0.76, while winter dropped to 0.31. Conversely, urban areas showed a higher winter correlation ($r = 0.71$ vs. 0.36 in summer). These results highlight two dynamics: (i) high summer temperatures and moderate winds cause localized impacts near sources (rural points), while (ii) efficient winter wind dispersion transports agricultural NH_3 further from sources, increasing its influence on urban centers.

3.3. $PM_{2.5}$ composition and time evolution

3.3.1. Average $PM_{2.5}$ composition

This section analyzes the $PM_{2.5}$ levels and composition from the rural site of Bujaraloz. Table 2 displays the average concentrations

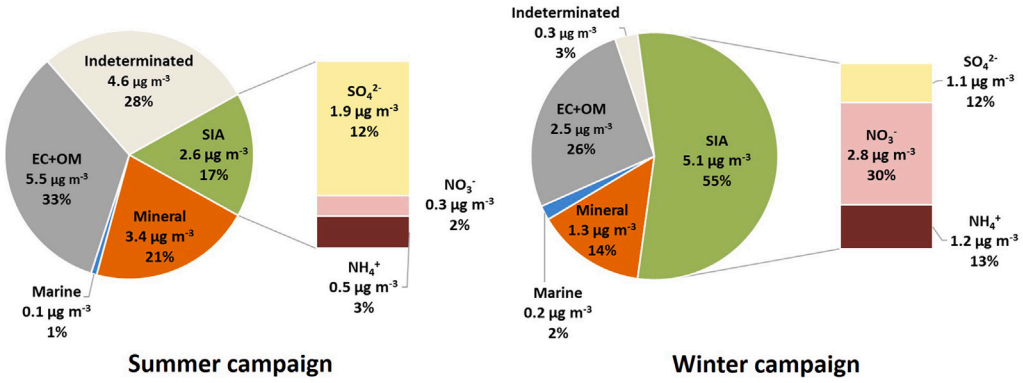

Fig. 3. Average levels and contributions to $PM_{2.5}$ compositions of elemental groupings in Bujaraloz during summer (7–22 July 2022) and winter (23 February–10 March 2023) campaigns. Due to their relationship with the presence of NH_3, the contributions of SIA have been broken down.

Table 2
Major components (in μg m^{-3}) of $PM_{2.5}$ in Bujaraloz during summer (7–22 July 2022) and winter (23 February–10 March 2023) campaigns.

	Summer campaign (N = 15)			Winter campaign (N = 15)		
	Average	Min.	Max.	Average	Min.	Max.
$PM_{2.5}$	16	11	24	9	3	18
OC	2.6	1.7	3.5	1.4	0.6	2.5
EC	0.2	0.1	0.3	0.2	<0.1	0.3
CO_3^{2-}	1.1	0.4	3.0	0.4	0.1	0.8
SiO_2	1.0	0.4	3.0	0.4	0.2	1.1
Al_2O_3	0.3	0.1	1.0	0.1	<0.1	0.4
Ca	0.7	0.2	2.0	0.2	<0.1	0.5
Fe	0.1	<0.1	0.3	<0.1	<0.1	0.1
K	0.2	0.1	0.3	0.1	<0.1	0.3
Mg	0.1	<0.1	0.3	<0.1	<0.1	<0.1
Na	0.1	0.1	0.1	<0.1	<0.1	0.1
SO_4^{2-}	1.9	1.4	2.8	1.1	0.3	2.2
NO_3^-	0.3	0.2	0.4	2.8	0.2	6.6
Cl	<0.1	<0.1	0.1	0.1	<0.1	0.2
NH_4^+	0.5	0.3	0.6	1.2	0.2	2.8
Mineral	**3.4**	**1.3**	**9.8**	**1.3**	**0.4**	**2.5**
Marine	**0.1**	**0.1**	**0.2**	**0.2**	<0.1	**0.3**
SIA	**2.6**	**2.0**	**3.6**	**5.1**	**0.8**	**11.3**
EC+OM	**5.5**	**3.6**	**7.1**	**2.5**	**1.0**	**4.5**
Indeterminate	**5.6**	**3.6**	**7.1**	**0.4**	<0.1	**1.1**

and major component ranges, while Fig. 3 illustrates the contribution of elemental groupings: (i) Secondary Inorganic Aerosols (SIA); (ii) Mineral Matter (CO_3^{2-} + SiO_2 + Al_2O_3 + Ca + Fe + K + Mg); (iii) Carbonaceous Matter (EC+OM); (iv) Marine Aerosols (Na + Cl; v) Indeterminate Fraction (primarily water and biases due to indirect calculations of, essentially, SiO_2 and OM).

Average winter $PM_{2.5}$ reached 9.3 μg m^{-3}, significantly lower than the summer average of 16.3 μg m^{-3}. Much of this difference is attributed to the indeterminate fraction, influenced by ambient humidity.

Relative contributions vary significantly by season. In winter, SIA was the dominant fraction (5.1 μg m^{-3}), accounting for 54% of average mass. In summer, its contribution dropped to 17% (2.6 μg m^{-3}), reflecting the instability of NH_4NO_3 at temperatures above 25–30°C. While SO_4^{2-} was higher in summer (1.9 vs. 1.1 μg m^{-3}), both NO_3^- and NH_4^+ peaked in winter (2.8 and 1.2 μg m^{-3}, respectively). These elevated winter SIA levels stem from high NH_3 inputs, lower volatilization, and atmospheric stability (specifically on March 4th and 5th) which favored photochemical accumulation. Background SIA levels in the CEV are nearly double those reported for the Montseny rural station in Catalonia (in't Veld et al., 2021).

Carbonaceous aerosols (EC+OM) comprised 33% of summer mass (5.5 μg m^{-3}) and 26% of winter mass (2.5 μg m^{-3}). As a rural site, EC constitutes less than 7% of this fraction. The OM fraction consists of secondary organic compounds from various precursors; summer levels were influenced by forest fires in the NE Iberian Peninsula (July 14–24), while winter levels likely included contributions from agricultural stubble burning. While EC levels at Bujaraloz are similar to Montseny, the OM fraction (3.2 μg m^{-3}) is notably higher than at the coastal station (in't Veld et al., 2021). OC/EC ratios were stable but higher in summer (14.3) than winter (8.3), indicating a low traffic contribution and consistent with rural background classifications where ratios typically range from > 15 in background sites to 1 in hotspots (Viana et al., 2006; Pey et al., 2009; Pio et al., 2011; Querol et al., 2013).

Primary (POA) and secondary organic aerosols (SOA) were estimated using the EC-tracer method (Turpin and Huntzicker, 1995). Assuming negligible primary biogenic POC in the fine fraction, SOA and POA were derived via:

$$SOA = OM - \left(\frac{OC}{EC}\right)_{prim} \cdot EC$$

$$POA = OM - SOA$$

The primary ratio $\left(\frac{OC}{EC}\right)_{prim}$ was estimated at 12.0 in summer and 7.5 in winter, using the median of the lowest 5% of ratios as in Escudero et al. (2015). These are high compared to urban values (1.0 in a Zaragoza traffic site or 2.6 at an industrial station in Monzón as shown in the latter study). Summer OM was dominated by the secondary fraction (57%) because Bujaraloz is exposed to long range transport and enhanced biogenic emissions activated by elevated temperatures, whereas POA was slightly dominant in winter (54%). The high winter POA proportion compared to sites like Montseny (74% SOA) suggests fine primary sources from local industry, such grain processing, or biomass use for domestic heating and stubble burning (Escudero et al., 2015).

The semi-arid nature of the CEV, combined with North African dust transport (Escudero et al., 2005), contributes to significant mineral matter levels. Although mineral matter is predominantly coarse, it accounted for 21% (3.4 μg m^{-3}) and 14% (1.3 μg m^{-3}) of summer and winter $PM_{2.5}$, respectively. Summer peaks were driven by a lack of precipitation and specific Saharan dust events (July 16–25). In contrast, winter rainfall and the absence of African air masses reduced these levels. Mineral matter in Bujaraloz is six times higher than at Montseny (in't Veld et al., 2021).

Marine aerosols were the least abundant (1%–2%), limited by the site's inland distance and the coarse nature of sea-salt particles.

The indeterminate fraction varied drastically, representing 28% of summer mass (4.6 μg m^{-3}) but only 3% in winter (0.3 μg m^{-3}). Analysis reveals a correlation with maximum relative humidity (RH) in Bujaraloz during summer (r = 0.58), excluding the final day when mineral dust arrival skewed the proportions (Figure S5).

Within Europe, recent urban measurements in northern France reported a mean $PM_{2.5}$ concentration of 12.6 ± 9.5 μg m^{-3}, with SIA

representing 36% of the mass (Allouche et al., 2024), highlighting the relevance of SIA in certain western European environments. Likewise, receptor modeling at urban background sites in Birmingham (UK) indicates present-day $PM_{2.5}$ levels around 7–8 μg m^{-3}, with ammonium nitrate contributing 20%–22% of $PM_{2.5}$ (Srivastava et al., 2025), emphasizing that nitrate-rich SIA remains a major fraction even under declining PM mass in the UK. Cesari et al. (2025) also reported $PM_{2.5}$ values in three sites in Italy ranging between 9–18 μg m^{-3}, with NO_3^- from 0.4 to 1.6 μg m^{-3}, and NH_4^+ from 0.2 to 0.4 μg m^{-3}. These European comparisons support that our observed $PM_{2.5}$ levels and the relative importance of SIA are consistent with the broader western European behavior, while also reflecting local conditions in our region.

At the global scale, $PM_{2.5}$ concentrations and composition can be substantially higher and compositionally different in major hotspot regions, particularly in South Asia. For example, an extensive seasonal campaign in Delhi–NCR (Bawase et al., 2021) reported $PM_{2.5}$ dominated by OM and SIA (around 41 and 31 μg m^{-3}, respectively), illustrating much heavier pollution burdens and strong secondary contributions compared with typical European sites. Global composition mapping further indicates that population-weighted $PM_{2.5}$ exposure is largely driven by particulate organic mass and SIA, with strong regional contrasts and particularly high secondary inorganic contributions over East China (Philip et al., 2014). Consistently, recent global assessments (Li et al., 2023; Tsimpidi et al., 2025) show that $PM_{2.5}$ exposure remains highest across parts of Asia, Africa and the Middle East, underscoring the strong global gradients in $PM_{2.5}$ levels.

3.3.2. Temporal evolution of $PM_{2.5}$ composition

The temporal variability of $PM_{2.5}$ and its components is illustrated in Fig. 4. In the summer campaign, concentrations trended upward. During the initial phase (July 8–11), levels remained below 15 μg m^{-3}, with carbonaceous matter (35%), the indeterminate fraction (34%), SIA (18%), and mineral matter (10%) dominating. This period featured westerly transport with higher wind speeds and lower temperatures. From July 12, mineral matter rose significantly (2.9–9.8 μg m^{-3}), peaking at 40% on July 22. This aligns with North African dust intrusions reported by MITERD (July 13–25). Carbonaceous aerosols also increased (4.4–7.1 μg m^{-3}), peaking on July 16 during regional biomass burning (July 14–24). Meanwhile, SIA remained stable (2.3–3.6 μg m^{-3}), reducing its relative weight to 16% and the indeterminate fraction dropped to 27% as southerly air masses decreased humidity and increased temperatures.

In the winter campaign, $PM_{2.5}$ increased progressively over the first 11 days (Feb 23–Mar 5). Early rainfall and subsequent weakening westerly winds limited pollutant dispersion. SIA dominated this phase (44%–67%), reaching exceptionally high levels for a rural site (7.6–11.3 μg m^{-3}) between March 2 and 5. Lighter winds and sunnier conditions during this window promoted ammonium nitrate formation and accumulation. A MITERD-reported biomass burning episode on March 5 further elevated SIA and carbonaceous matter (peaking at 4.5 μg m^{-3}). Mineral matter fluctuated between 10% and 20%, peaking on February 23 due to the end of an African dust episode. From March 6 to 9, shifting southwesterly winds brought warmer air, causing SIA to decline (20%–45%) while the relative weights of carbonaceous, mineral, and indeterminate fractions increased. Notably, the winter indeterminate fraction was consistently low, averaging only 0.2 μg m^{-3} (3%).

3.4. Exploratory $PM_{2.5}$ source apportionment

The five-factor PMF solution identifies one natural source, mineral dust from Saharan outbreaks, and four anthropogenic sources, comprising two primary and two secondary aerosol factors (Fig. 5).

Winter secondary inorganic aerosol (ammonium nitrate type). Dominated by NO_3^- and NH_4^+, this factor reflects ammonium nitrate formation during stagnant, low-temperature periods (Pey et al., 2010). The presence of EC, OC, K, and trace metals (Zn, Sn, Cd, Pb) indicates mixed combustion from traffic, industry, and biomass burning (Salameh et al., 2018). Absent in summer, it peaked in early March 2023, accounting for nearly half of winter $PM_{2.5}$ (Fig. 6).

Summer secondary aerosols. The chemical profile of this PMF factor is defined by OC, SO_4^{-2} and NH_4^+. However, these compounds are not dominantly explicated by this factor, but distributed along the five PMF factors. On the contrary, V and Ni are dominantly explained in this factor. The enhanced presence of V and Ni under southerly and south-easterly winds (see Section 3.1) suggests an influence from fuel-oil combustion, possibly related to shipping or industrial activities taking place over the Mediterranean (Pey et al., 2013). With this in mind, and considering the intense ageing of air masses in summer in the Western Mediterranean, the factor could represent a mixture of secondary organics and sulphate from different sources. The factor dominates secondary aerosols in summer (Fig. 6), on average 3.0 μg m^{-3}, with reduced concentrations during the winter campaign (0.5 μg m^{-3}).

Regional-local dust. Characterized by mineral signatures enriched in Ca, Mg, SO_4^{-2}, and Na, plus trace metals (Cu, Zn, Cd, Sb, Pb), this factor represents regional dust from Ebro Valley soils and saline surfaces. It likely includes a road dust component (Amato et al., 2016). Contributions were higher and more consistent in summer (3.3 μg m^{-3} average) than in winter (1.1 μg m^{-3}), though a wind-driven peak of 5.0 μg m^{-3} occurred on February 22nd.

Mineral with saharan dust. Strongly enriched in crustal elements (Al, Ca, Fe, Mg, Li, Ti, Sr, Ga, La), this factor accounts for 47%–70% of their variance. It was the most abundant summer source (3.8 μg m^{-3} average) due to frequent Saharan outbreaks (Section 3.3.2), contrasting sharply with the winter average (0.5 μg m^{-3}).

Industrial agricultural. This source is enriched in OC, EC, mineral components, Cl^-, and P, suggesting either industrial forage dehydration or biomass burning (Salameh et al., 2018). Its contribution was higher in winter (2.4 μg m^{-3}) than summer (1.5 μg m^{-3}), aligning with permitted biomass burning periods. Summer activity likely stems from industrial drying processes or sporadic forest fire emissions.

4. Concluding remarks and future research

This study characterizes the chemical composition, formation pathways, and source attribution of $PM_{2.5}$ at a major NH_3 hotspot in the Central Ebro Valley (CEV), providing empirical evidence that intensive livestock emissions are the primary driver of regional particulate pollution through intensive monitoring campaigns during contrasting climatic periods. These results also highlight the significant impacts of biomass burning and the resuspension of mineral matter associated with agricultural practices.

Our findings reveal that the CEV functions as a massive atmospheric reservoir for the transport of ammonia to the Northern and Eastern Iberian Peninsula and the Mediterranean Basin. This high ammonia availability in the CEV maximizes the conversion of nitric acid into particulate NH_4NO_3. This species is the single largest contributor to $PM_{2.5}$ mass during winter, accounting for up to 54% of the total load. This fraction drops to 17% in summer due to high temperatures promoting the volatilization of ammonium nitrate.

A seasonal paradox emerges regarding NH_3 levels. Despite higher potential emissions in summer due to elevated temperatures, surface NH_3 concentrations remain comparable to or lower than winter levels. This is attributed to the deep development of the Planetary Boundary Layer (PBL) in summer, which promotes vertical mixing and dilutes precursors. Conversely, winter conditions combine lower PBL

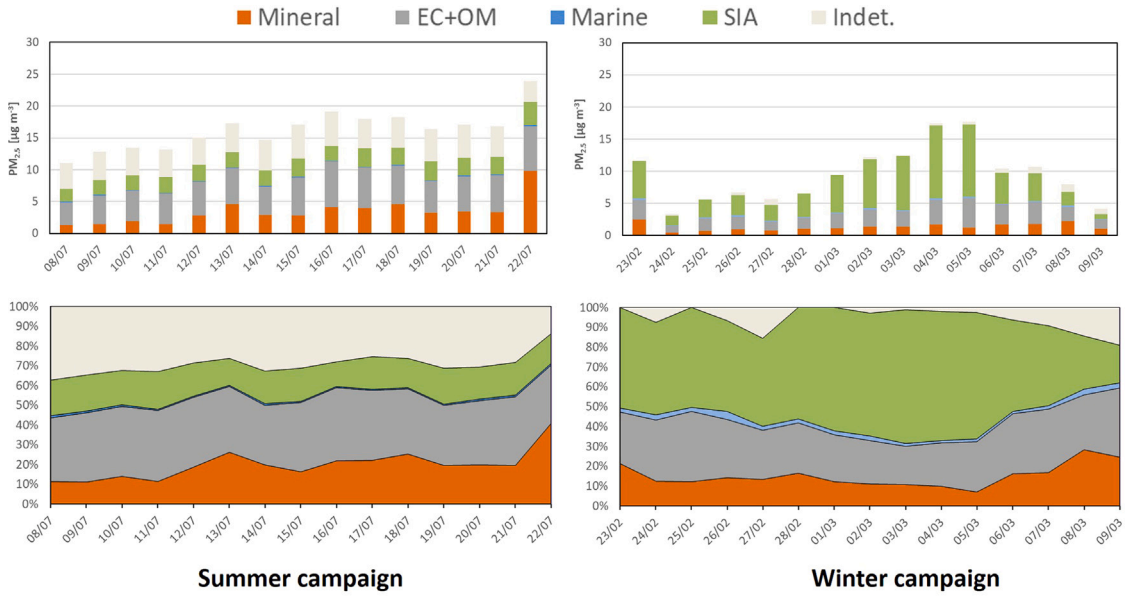

Fig. 4. Temporal evolution of concentrations (upper figures) and relative contributions (lower figures) of element groups to the composition of $PM_{2.5}$ in Bujaraloz during summer (7–22 July 2022) and winter (23 February–10 March 2023) campaigns.

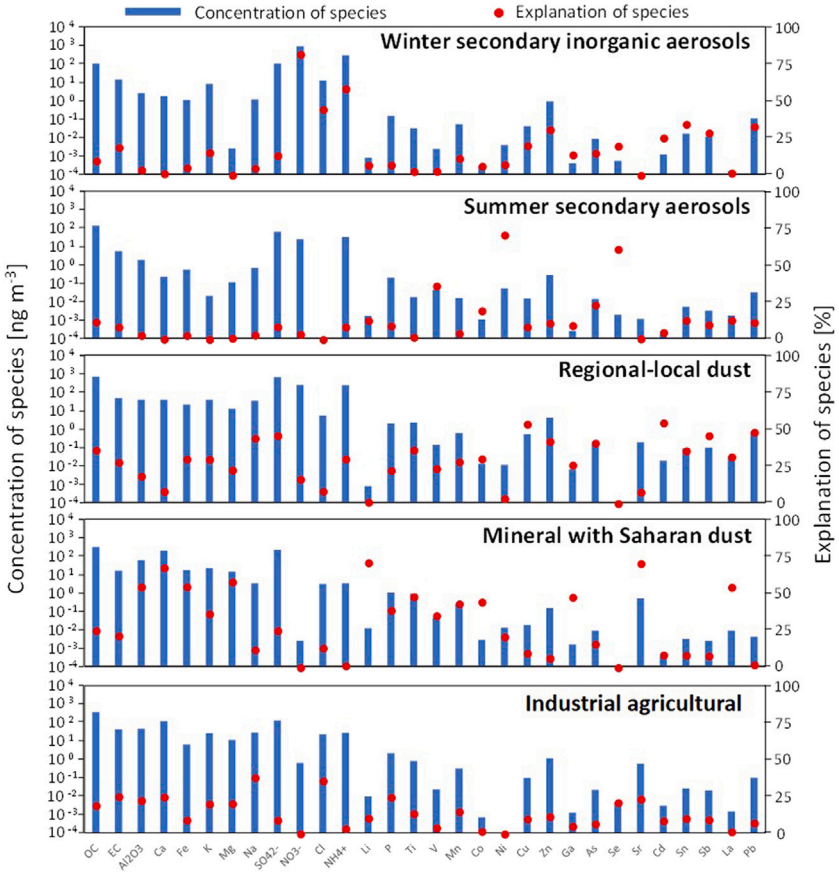

Fig. 5. Chemical profiles of the five-factor PMF solution. For each factor, blue bars show the species concentration (in ng m^{-3}) and red circles display the percentage of each species explained by the factor (%). (For interpretation of the references to color in this figure legend, the reader is referred to the web version of this article.)

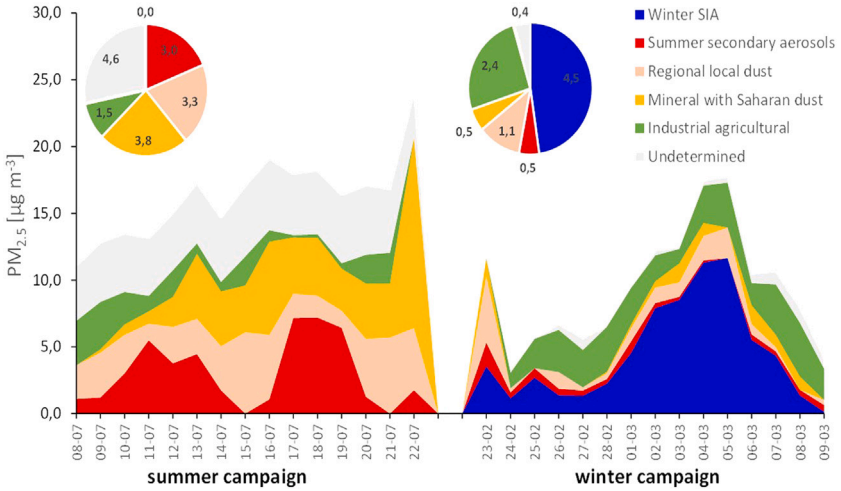

Fig. 6. Temporal variation of daily $PM_{2.5}$ contributions (in µg m^{-3}) of each of the five factors retrieved by PMF for the summer and winter campaigns. Pie charts for the summer and winter campaigns indicating average values of each PMF factor.

heights, stagnant air, and temperature inversions to create a pollution-amplifying effect, further aided by the semi-volatile nature of NH_4NO_3 which favors particle formation at lower temperatures.

Exploratory source contribution analysis via the PMF model identified five factors with marked seasonality. Two sources were identified associated with secondary aerosols likely driven by agro-livestock activity being one of the dominant factor in winter, two mineral factors related to local tilling and Saharan dust (dominant in summer), and an industrial factor linked to agricultural product processing exerts a consistent impact throughout the year.

These findings suggest that $PM_{2.5}$ mitigation strategies must prioritize the control of NH_3 as the area's most abundant precursor, especially in winter when SIA production is most stable. This requires strict measures in agricultural and livestock management, such as optimized manure storage, low-emission housing, and rapid fertilizer incorporation. Additionally, the study emphasizes the need to address organic compound emissions, as carbonaceous aerosols stem from a complex mixture of residential, agricultural, and industrial activities. Reducing NH_3 offers the collateral benefit of protecting human health while preventing the eutrophication and acidification of ecosystems caused by nitrogen deposition.

Future research should extend monitoring periods to execute more robust source contribution analyses and focus on year-round NH_3 contamination using both surface and satellite measurements to derive equivalent surface concentration factors. High-level scientific equipment should be deployed in specific campaigns to discern real-time PM speciation and the influence of meteorological factors like PBL height. Furthermore, Chemical Transport Models are necessary to interpret transport and deposition mechanisms, using the conclusions of this work to validate and optimize model performance. Ultimately, transitioning from traditional NO_x/SO_2 controls to mandatory, stringent NH_3 emission limits for the agricultural sector is the only viable path to achieving clean air standards in such heavily agriculturalized regions.

CRediT authorship contribution statement

Miguel Escudero: Writing – review & editing, Writing – original draft, Visualization, Supervision, Resources, Project administration, Methodology, Funding acquisition, Formal analysis, Conceptualization. **Natividad Miguel:** Writing – review & editing, Supervision, Resources, Project administration. **José Hernández de la Torre:** Writing – review & editing, Visualization, Resources, Methodology, Formal analysis. **Miguel Arner:** Writing – review & editing, Resources, Formal analysis. **Julia Marín-Sáez:** Writing – review & editing, Resources. **Juan Hierro:** Writing – review & editing, Resources. **Andrés Alastuey:** Writing – review & editing, Investigation. **Xavier Querol:** Writing – review & editing, Investigation. **Cristina Reche:** Writing – review & editing, Investigation. **Amalia Muñoz:** Writing – review & editing, Investigation. **Esther Borrás:** Investigation. **Jorge Pey:** Writing – review & editing, Visualization, Formal analysis.

Declaration of Generative AI and AI-assisted technologies in the writing process

During the preparation of this work the author(s) used Gemini in order to proofread and correct written English. After using this tool/service, the author(s) reviewed and edited the content as needed and take(s) full responsibility for the content of the published article.

Declaration of competing interest

The authors declare the following financial interests/personal relationships which may be considered as potential competing interests: Miguel Escudero reports financial support was provided by Government of Aragón. Miguel Escudero reports financial support was provided by European Regional Development Fund. Miguel Escudero reports was provided by State Agency of Research Spain. If there are other authors, they declare that they have no known competing financial interests or personal relationships that could have appeared to influence the work reported in this paper.

Acknowledgments

This research was financially supported by the Government of Aragón (contracts OTRI 2022/0350 and 2023/0105; E02_23R project), the Spanish Ministry of Science, Innovation and Universities (projects PID2022-142160OB-I00 and AIA2025-163866-C22), and the Programme Interreg POCTEFA 2021–2027 (project EFA 210/06/ECOAIR) with co-financing of the European Regional Development Funds (ERDF). The authors are grateful for the collaboration and assistance provided by the personnel from the Environment Laboratory of the Diputación Provincial de Teruel, J. Aguirre S.L., and the General Direction of Environmental Education of the Government of Aragón.

Appendix A. Supplementary data

Supplementary material related to this article can be found online at https://doi.org/10.1016/j.envpol.2026.128232.

Data availability

Data will be made available on request.

References

Al-Thani, H., Koç, M., Isaifan, R.J., 2018. A review on the direct effect of particulate atmospheric pollution on materials and its mitigation for sustainable cities and societies. Environ. Sci. Pollut. Res. 25, 27839–27857. http://dx.doi.org/10.1007/s11356-018-2952-8.

Allouche, Y., Fadel, M., Ferté, A., Verdin, A., Ledoux, F., Courcot, D., 2024. Phenomenology of the composition of $PM_{2.5}$ at an urban site in Northern France. Atmosphere 15 (5), 603. http://dx.doi.org/10.3390/atmos15050603.

Amato, F., Alastuey, A., Karanasiou, A., Lucarelli, F., Nava, S., Calzolai, G., Severi, M., Becagli, S., Gianelle, V.L., Colombi, C., Alves, C., Custódio, D., Nunes, T., Cerqueira, M., Pio, C., Eleftheriadis, K., Diapouli, E., Reche, C., Minguillón, M.C., Manousakas, M.-I., Maggos, T., Vratolis, S., Harrison, R.M., Querol, X., 2016. AIRUSE-LIFE+: a harmonized PM speciation and source apportionment in five southern European cities. Atmospheric Chem. Phys. 16, 3289–3309. http://dx.doi.org/10.5194/acp-16-3289-2016.

Bawase, M., Sathe, Y., Khandaskar, H., Thipse, S., 2021. Chemical composition and source attribution of $PM_{2.5}$ and PM_{10} in Delhi–National Capital Region (NCR) of India: Results from an extensive seasonal campaign. J. Atmos. Chem. 78, 35–58. http://dx.doi.org/10.1007/s10874-020-09412-7.

Beck, H.E., Zimmermann, N.E., McVicar, T.R., Vergopolan, N., Berg, A., Wood, E.F., 2018. Present and future Köppen-Geiger climate classification maps at 1-km resolution. Sci. Data 5, 180214. http://dx.doi.org/10.1038/sdata.2018.214.

Behera, S.N., Sharma, M., 2012. Transformation of atmospheric ammonia and acid gases into components of $PM_{2.5}$: An environmental chamber study. Environ. Pollut. 166, 204–211. http://dx.doi.org/10.1007/s11356-011-0635-9.

Belis, C.A., Larsen, B., Amato, F., El Haddad, I., Favez, O., Harrison, R.M., Hopke, P.K., Nava, S., Paatero, P., Prévot, A., Quass, U., Vecchi, R., Viana, M., 2014. European Guide on Air Pollution Source Apportionment with Receptor Models. Publication Office of the European Union, Italy, p. 88, http://source-apportionment.jrc.ec.europa.eu/Docu/EU_guide_on_SA.pdf.

Bell, M.L., Ebisu, K., Leaderer, B.P., Gent, J.F., Lee, H.J., Koutrakis, P., Wang, Y., Dominici, F., Peng, R.D., 2014. Associations of $PM_{2.5}$ constituents and sources with hospital admissions: analysis of four counties in connecticut and massachusetts (USA) for persons $\geq$ 65 years of age. Environ. Health Perspect. 122, 138–144. http://dx.doi.org/10.1289/ehp.1306656.

Best Rogowski, C. B, Bredell, C., Shi, Y., Tien-Smith, A., Szybka, M., Fung, K.W., Hong, L., Phillips, V., Jovanovic Andersen, Z., Sharp, S.J., Woodcock, J., Brayne, C., Navaratnam, A., Khreis, H., 2025. Long-term air pollution exposure and incident dementia: a systematic review and meta-analysis. Lancet Planet. Health 9 (7), http://dx.doi.org/10.1016/S2542-5196(25)00118-4.

Cesari, D., Mapelli, C., Dinoi, A., Chirizzi, D., Pennetta, A., Deluca, G., De Benedetto, G.E., Contini, D., 2025. Characterization of $PM_{2.5}$ and its oxidative potential in three areas of Southern Italy. Atmos. Environ. 350, 121146.

Chen, G., Canonaco, F., Tobler, A., Aas, W., Alastuey, A., Allan, J., Atabakhsh, S., Aurela, M., Baltensperger, U., Bougiatioti, A., De Brito, J.F., Ceburnis, D., Chazeau, B., Chebaicheb, H., Daellenbach, K.R., Ehn, M., Haddad, I.El., Eleftheriadis, O., Flentje, H., Font, A., Fossum, K., Freney, M., Green, M.C., Heikkinen, L., Herrmann, H., Kalogridis, A.C., Keernik, R., Lin, C., Lunder, C., Maasikmets, M., Manousakas, M.I., Marchand, N., Marin, C., Marmureanu, L., Mihalopoulos, N., Močnik, G., Nęcki, J., O'Dowd, C., Ovadnevaite, J., Peter, T., Petit, J.E., Pikridas, M., Platt, S.M., Pokorná, P., Poulain, L., Priestman, M., Riffault, V., Rinaldi, M., Rózański, K., Schwarz, J., Sciare, J., Simon, L., Skiba, A., Slowik, J.G., Sosedova, Y., Stavroulas, I., Styszko, K., Teinemaa, E., Timonen, H., Tremper, A., Vasilescu, J., Via, M., Vodička, P., Wiedensohler, A., Zografou, O., Minguillón, M.C., Prévôt, A.S.H., 2022. European aerosol phenomenology - 8: Harmonised source apportionment of organic aerosol using 22 year-long ACSM/AMS datasets. Environ. Int. 166, 107325. http://dx.doi.org/10.1016/j.envint.2022.107325.

Clarisse, L., Clerbaux, C., Dentener, F., Hurtmans, D., Coheur, P.F., 2009. Global ammonia distribution derived from infrared satellite observations. Nat. Geosci. 2, 479–483. http://dx.doi.org/10.1038/ngeo551.

Cuadrat, J.M., 2004. El clima de aragón. In: Peña, J.L., Longares, L.A., Sánchez, M. (Eds.), Geografía Física de Aragón. Aspectos generales y temáticos. Universidad de Zaragoza e Institución Fernando el Católico, Zaragoza, p. 343.

Daellenbach, K.R., Uzu, G., Jiang, J., Cassagnes, L.-E., Leni, Z., Vlachou, A., Stefenelli, G., Canonaco, F., Weber, S., Segers, A., Kuenen, J.J.P., Schaap, M., Favez, O., Albinet, A., Aksoyoglu, S., Dommen, J., Baltensperger, U., Geiser, M., El Haddad, I., Jaffrezo, J.-L., Prévôt, A.S.H., 2020. Sources of particulate-matter air pollution and its oxidative potential in Europe. Nature 587, 414–419. http://dx.doi.org/10.1038/s41586-020-2902-8.

Dammers, E., McLinden, C.A., Griffin, D., Shephard, M.W., Van Der Graaf, S., Lutsch, E., Schaap, M., Gainairu-Matz, Y., Fioletov, V., Van Damme, M., Whitburn, S., Clarisse, L., Cady-Pereira, K., Clerbaux, C., Francois Coheur, P., Erisman, J.W., 2019. NH_3 emissions from large point sources derived from CrIS and IASI satellite observations. Atmospheric Chem. Phys. 19, 12261–12293. http://dx.doi.org/10.5194/acp-19-12261-2019.

Domínguez, B., Nicolás, J.F., Mantilla, E., Gimeno, C., Borrás, E., Ródenas, M., Vera, T., Soler, R., Alfosea Simón, M., Yubero, E., Crespo, J., Galindo, N., Clemente, A., Muñoz, A., 2025. Estimation of light absorption by secondary brown carbon during agricultural residues burning. Atmos. Res. 325, 108239. http://dx.doi.org/10.1016/j.atmosres.2025.108239.

EEA, 2025. Emissions of the main air pollutants in Europe. http://dx.doi.org/10.2800/2805780, https://www.eea.europa.eu/en/analysis/publications/air-pollution-in-europe-2025-reporting-status-under-the-national-emission-reduction-commitments-directive. (Last Access 8 October 2025), ISBN: 978-92-9480-722-9, ISSN: 2467-3196.

Ehrnsperger, L., Klemm, O., 2021. Source apportionment of urban ammonia and its contribution to secondary particle formation in a mid-size European city. Aerosol Air Qual. Res. 21, 20040. http://dx.doi.org/10.4209/aaqr.2020.07.0404.

Escudero, M., Castillo, S., Querol, X., Avila, A., Alarcón, M., Viana, M.M., Alastuey, A., Cuevas, E., Rodríguez, S., 2005. Wet and dry African dust episodes over eastern Spain. J. Geophys. Res. 110, D18S08. http://dx.doi.org/10.1029/2004JD004731.

Escudero, M., Lozano, A., Hierro, J., del Valle, J., Mantilla, E., 2014. Urban influence on increasing ozone concentrations in a characteristic Mediterranean agglomeration. Atmos. Environ. 99, 322–332. http://dx.doi.org/10.1016/j.atmosenv.2014.09.061.

Escudero, M., Viana, M., Querol, X., Alastuey, A., Díez Hernández, P., García Dos Santos, S., Anzano, J., 2015. Industrial sources of primary and secondary organic aerosols in two urban environments in Spain. Environ. Sci. Pollut. Res. 22, 10413–10424. http://dx.doi.org/10.1007/s11356-015-4228-x.

Font, A., de Brito, J.F., Riffault, V., Conil, S., Jaffrezo, J.L., Bourin, A., 2024. Calculations of the conversion factor from organic carbon to organic matter for aerosol mass balance. Atmospheric Pollut. Res. 15 (12), 102301. http://dx.doi.org/10.1016/j.apr.2024.102301.

Fowler, D., Steadman, C.E., Stevenson, D., Coyle, M., Rees, R.M., Skiba, U.M., Sutton, M.A., Cape, J.N., Dore, A.J., Vieno, M., Simpson, D., Zaehle, S., Stocker, B.D., Rinaldi, M., Facchini, M.C., Flechard, C.R., Nemitz, E., Twigg, M., Erisman, J.W., Butterbach-Bahl, K., Galloway, J.N., 2015. Effects of global change during the 21st century on the nitrogen cycle. Atmospheric Chem. Phys. 15 (24), 13849–13893. http://dx.doi.org/10.5194/acp-15-13849-2015.

Frey, H.C., 2018. Trends in onroad transportation energy and emissions. J. Air Waste Manage. Assoc. 68, 514–563. http://dx.doi.org/10.1080/10962247.2018.1454357.

Government of Aragón, 2015. Order of 13 de febrero de 2015, de los consejeros de obras públicas, urbanismo, vivienda y transportes, de política territorial e interior, y de agricultura, ganadería y medio ambiente, por la que se sustituyen varios anexos de las directrices sectoriales sobre actividades e instalaciones ganaderas, cuya revisión se aprobó por el decreto 94/2009, de 26 de mayo, del gobierno de aragón. Bol. Of. Aragón 55.

Hime, N.J., Marks, G.B., Cowie, C.T., 2018. A comparison of the health effects of ambient particulate matter air pollution from five emission sources. Int. J. Environ. Res. Public Health 15, 1–24. http://dx.doi.org/10.3390/ijerph15061206.

Hopke, P.K., Querol, X., 2022. Is improved vehicular NOx control leading to increased urban NH_3 emissions? Environ. Sci. Technol. 56 (17), 11926–11927. http://dx.doi.org/10.1021/acs.est.2c04996.

INAGA, 2022. Explotaciones ganaderas. https://aplicaciones.aragon.es/inagisweb/visor_granjas. (Accessed 25 November 2022).

in't Veld, M., Alastuey, A., Pandolfi, M., Amato, F., Perez, N., Reche, C., Via, M., Minguillón, M.C., Escudero, M., Querol, X., 2021. Compositional changes of $PM_{2.5}$ in NE Spain during 2009–2018: a trend analysis of the chemical composition and source apportionment. Sci. Total Environ. 795, 148728. http://dx.doi.org/10.1016/j.scitotenv.2021.148728.

IPCC, 2023. Climate change 2023: Synthesis report. In: Core Writing Team, Lee, H., Romero, J. (Eds.), Contribution of Working Groups I, II and III To the Sixth Assessment Report of the Intergovernmental Panel on Climate Change. IPCC, Geneva, Switzerland, p. 184. http://dx.doi.org/10.59327/IPCC/AR6-9789291691647.

Jiang, H., Jang, M., Sabo-Attwood, T., Robinson, S.E., 2016. Oxidative potential of secondary organic aerosols produced from photooxidation of different hydrocarbons using outdoor chamber under ambient sunlight. Atmos. Environ. 131, 382–389. http://dx.doi.org/10.1016/j.atmosenv.2016.02.016.

Kelly, F.J., Fussell, J.C., 2012. Size, source and chemical composition as determinants of toxicity attributable to ambient particulate matter. Atmos. Environ. 60, 504–526. http://dx.doi.org/10.1016/j.atmosenv.2012.06.039.

Li, C., van Donkelaar, A., Hammer, M.S., McDuffie, E.E., Burnett, R.T., Spadaro, J.V., Chatterjee, D., Cohen, A.J., Apte, J.S., Southerland, V.A., Anenberg, S.C., Brauer, M., Martin, R.V., 2023. Reversal of trends in global fine particulate matter air pollution. Nat. Commun. 14, 5349. http://dx.doi.org/10.1038/s41467-023-41086-z.

Liu, X., Lara, R., Dufresne, M., Wu, L., Wang, T., Monge, M., Reche, C., Di Leo, A., Lanzani, G., Colombi Font, A., Sheehan, A., Green, D.C., Makkonen, U., Sauvage, S., Salameh, T., Petit, J.E., Chatain, M., Coe, H., Hou, S., Harrison, R., Hopke, P.K., Petäjä, T., Alastuey, A., Querol, X., 2024. Variability of ambient air ammonia in urban Europe (Finland, France, Italy, Spain, and the UK). Environ. Int. 185, 108519. http://dx.doi.org/10.1016/j.envint.2024.108519.

Liu, L., Zhang, X., Wong, A.Y.H., Xu, W., Liu, X., Li, Y., Mi, H., Lu, X., Zhao, L., Wang, Z., Wu, X., Wei, J., 2019. Estimating global surface ammonia concentrations inferred from satellite retrievals. Atmospheric Chem. Phys. 19 (18), 12051–12066. http://dx.doi.org/10.5194/acp-19-12051-2019.

Malherbe, L., German, R., Couvidat, F., Zanatta, L., Blannin, L., James, A., Lètinois, L., Schucht, S., Berthelot, B., Raoult, J., 2022. Emissions of Ammonia and Methane from the Agricultural Sector. Emissions from Livestock Farming. Eionet Report - ETCHE 2022/21, European Topic Centre on Human Health and the Environment.

Manninen, M., Jääskeläinen, K., Stephens, A., Iwanicka, A., Tang, S., van Dijk, N., 2023. NH_3 concentrations below the current critical level affect the epiphytic macrolichen communities – Evidence from a Northern European City. Sci. Total Environ. 877, 162877. http://dx.doi.org/10.1016/j.scitotenv.2023.162877.

Ministerio para la Transición Ecológica y el Reto Demográfico, 2025. Informative Inventory Report of Pollutant Emissions Into the Atmosphere. MITECO, Centro de Publicaciones, Available at: https://www.miteco.gob.es/content/dam/miteco/es/calidad-y-evaluacion-ambiental/temas/sistema-espanol-de-inventario-sei-/es-iir-edicion-2025.pdf.

Nair, A.A., Yu, F., 2020. Quantification of atmospheric ammonia concentrations: A review of its measurement and modeling. Atmosphere 11 (10), 1092. http://dx.doi.org/10.3390/atmos11101092.

Naseem, S., King, A.J., 2018. Ammonia production in poultry houses can affect health of humans, birds, and the environment—techniques for its reduction during poultry production. Environtal Sci. Pollut. Res. 25, 15269–15293. http://dx.doi.org/10.1007/s11356-018-2018-y.

Paatero, P., Tapper, U., 1994. Positive matrix factorization: a non-negative factor model with optimal utilization of error estimates of data values. Environmetrics 5, 111–126. http://dx.doi.org/10.1002/env.3170050203.

Park, M., Joo, H.S., Lee, K., Jang, M., Kim, S.D., Kim, I., Borlaza, L.J.S., Lim, H., Shin, H., Chung, K.H., Choi, Y.H., Park, S.G., Bae, M.S., Lee, J., Song, H., Park, K., 2018. Differential toxicities of fine particulatematters from various sources. Sci. Rep. 8, 1–11. http://dx.doi.org/10.1038/s41598-018-35398-0.

Peña, J.L., Lozano, M.V., 2004. Las unidades del relieve aragonés. In: Peña, J.L., Longares, L.A., Sánchez, M. (Eds.), Geografía Física de Aragón. Aspectos generales y temáticos. Universidad de Zaragoza e Institución Fernando el Católico, Zaragoza, p. 343.

Pey, J., Pérez, N., Castillo, S., Viana, M., Moreno, T., Pandolfi, M., López-Sebastián, J.M., Alastuey, A., Querol, X., 2009. Geochemistry of regional background aerosols in the western Mediterranean. Atmos. Res. 94, 422–435. http://dx.doi.org/10.1016/j.atmosres.2009.07.001.

Pey, J., Pérez, N., Cortés, J., Alastuey, A., Querol, X., 2013. Chemical fingerprint and impact of shipping emissions over a western Mediterranean metropolis: primary and aged contributions. Sci. Total Environ. 463–464, 497–507. http://dx.doi.org/10.1016/j.scitotenv.2013.06.061.

Pey, J., Pérez, N., Querol, X., Alastuey, A., Cusack, M., Reche, C., 2010. Intense winter atmospheric pollution episodes affecting the western Mediterranean. Sci. Total Environ. 408 (8), 1951–1959. http://dx.doi.org/10.1016/j.scitotenv.2010.01.052.

Philip, S., Martin, R.V., Donkelaar, A.van., Lo, J.W.-H., Wang, Y., Chen, D., Zhang, L., Kasibhatla, P.S., Wang, S., Zhang, Q., Lu, Z., Streets, D.G., Bittman, S., Macdonald, D.J., 2014. Global chemical composition of ambient fine particulate matter for exposure assessment. Environ. Sci. Technol. http://dx.doi.org/10.1021/es502965b.

Pio, C., Cerqueira, M., Harrison, R.M., Nunes, T., Mirante, F., Alves, C., Oliveira, C., Sánchez de la Campa, A., Artíñano, B., Matos, M., 2011. OC/EC ratio observations in Europe: re-thinking the approach for apportionment between primary and secondary organic carbon. Atmos. Environ. 45, 6121–6132. http://dx.doi.org/10.1016/j.atmosenv.2011.08.045.

Querol, X., Alastuey, A., Pandolfi, M., Reche, C., Pérez, N., Minguillón, M.C., Moreno, T., Viana, M., Escudero, M., Orio, A., Pallarés, M., Reina, F., 2014. 2001–2012 trends on air quality in Spain. Sci. Total Environ. 490, 957–969. http://dx.doi.org/10.1016/j.scitotenv.2014.05.074.

Querol, X., Alastuey, A., Viana, M., Moreno, T., Reche, C., Minguillón, M.C., Ripoll, A., Pandolfi, M., Amato, F., Karanasiou, A., Perez, N., Pey, J., Cusack, M., Vázquez, R., Plana, F., Dall'Osto, M., de la Rosa, J., Sánchez de la Campa, A., Fernández-Camacho, R., Rodríguez, S., Pio, C., Alados-Arboledas, L., Titos, G., Artíñano, B., Salvador, P., García dos Santos, S., Fernández Patier, R., 2013. Variability of carbonaceous aerosols in remote, rural, urban and industrial environments in Spain: implications for air quality policy. Atmospheric Chem. Phys. 13, 6185–6206. http://dx.doi.org/10.5194/acp-13-6185-2013.

Rai, P.K., 2016. Impacts of particulate matter pollution on plants: Implications for environmental biomonitoring. Ecotoxicol. Environ. Safety 129, 120–136. http://dx.doi.org/10.1016/j.ecoenv.2016.03.012.

Reche, C., Perez, N., Alastuey, A., Cots, N., Pérez, E., Querol, X., 2022. 2011–2020 trends of urban and regional ammonia in and around Barcelona, NE Spain. Chemosphere 304, 135347. http://dx.doi.org/10.1016/j.chemosphere.2022.135347.

Reche, C., Viana, M., Karanasiou, A., Cusack, M., Alastuey, A., Artíñano, B., Revuelta, M.A., López-Mahía, P., Blanco-Heras, G., Rodríguez, S., Sánchez de la Campa, A.M., Fernández-Camacho, R., González-Castanedo, Y., Mantilla, E., Tang, Y.S., Querol, X., 2015. Urban NH_3 levels and sources in six major Spanish cities. Chemosphere 119, 769–777. http://dx.doi.org/10.1016/j.chemosphere.2014.07.097.

Reche, C., Viana, M., Pandolfi, M., Alastuey, A., Moreno, T., Amato, F., Ripoll, A., Querol, X., 2012. Urban NH_3 levels and sources in a Mediterranean environment. Atmospheric Environ. 57, 153–164. http://dx.doi.org/10.1016/j.atmosenv.2012.04.021, 1994.

Saiz-Lopez, A., Borge, R., Notario, A., Adame, J.A., La Paz, D.D., Querol, X., Artíñano, B., Gómez-Moreno, F.J., Cuevas, C.A., 2017. Unexpected increase in the oxidation capacity of the urban atmosphere of Madrid, Spain. Sci. Rep. 7, 1–11. http://dx.doi.org/10.1038/srep45956.

Salameh, D., Pey, J., Bozzetti, C., Haddad, I.El., Detournay, A., Sylvestre, A., Canonaco, F., Armengaud, A., Piga, D., Robin, D., Prevot, A.S.H., Jaffrezo, J.-L., Wortham, H., Marchand, N., 2018. Sources of $PM_{2.5}$ at an urban-industrial Mediterranean city, Marseille (France): application of the ME-2 solver to inorganic and organic markers. Atmos. Res. 214, 263–274. http://dx.doi.org/10.1016/j.atmosres.2018.08.005.

Schwab, J.J., Li, Y., Bae, M.S., Demerjian, K.L., Hou, J., Zhou, X., Jensen, B., Pryor, S.C., 2007. A laboratory intercomparison of Real-Time gaseous ammonia measurement methods. Environ. Sci. Technol. 41 (24), 8412–8419. http://dx.doi.org/10.1021/es070354r.

Srivastava, D., Saksakulkrai, S., Acton, W.J.F., Rooney, D.J., Hall, J., Hou, S., Wolstencroft, M., Bartington, S., Harrison, R.M., Shi, Z., Bloss, W.J., 2025. Comparative receptor modelling for the sources of fine particulate matter ($PM_{2.5}$) at urban sites in the UK. Atmos. Environ. 343, 120963. http://dx.doi.org/10.1016/j.atmosenv.2024.120963.

Sutton, M.A., Erisman, J.W., Dentener, F., Möller, D., 2008. Ammonia in the environment: from ancient times to the present Review Article. Environ. Pollut. 156, 583–604.

Tang, Y.S., Cape, J.N., Sutton, M.A., 2001. Development and types of passive samplers for monitoring atmospheric NO_2 and NH_3 concentrations. In: Proceedings of the International Symposium on Passive Sampling of Gaseous Pollutants in Ecological Research. Vol. 1, TheScientificWorld, pp. 513–529.

Tichý, O., Eckhardt, S., Balkanski, Y., Hauglustaine, D., Evangeliou, N., 2023. Decreasing trends of ammonia emissions over Europe seen from remote sensing and inverse modelling. Amospheric Chem. Phys. 23 (24), 15235–15252. http://dx.doi.org/10.5194/acp-23-15235-2023.

Tsimpidi, A.P., Scholz, S.M.C., Milousis, A., Mihalopoulos, N., Karydis, V.A., 2025. Aerosol composition trends during 2000–2020: In-depth insights from model predictions and multiple worldwide near-surface observation datasets. Atmospheric Chem. Phys. 25, 10183–10213. http://dx.doi.org/10.5194/acp-25-10183-2025.

Turpin, B.J., Huntzicker, J.J., 1995. Identification of secondary organic aerosol episodes and quantitation of primary and secondary organic aerosol concentrations during SCAQS. Atmos. Environ. 29, 3527–3544.

Twigg, M.M., Berkhout, A.J., Cowan, N., Crunaire, S., Dammers, E., Ebert, V., Gaudion, V., Haaima, M., Häni, C., John, L., Jones, M.R., Kamps, B., Kentisbeer, J., Kupper, T., Leeson, S.R., Leuenberger, D., Lüttschwager, N.O.B., Makkonen, U., Martin, N.A., Missler, D., Mounsor, D., Neftel, A., Nelson, C., Nemitz, E., Oudwater, R., Pascale, C., Petit, J.-E., Pogany, A., Redon, N., Sintermann, J., Stephens, A., Sutton, M.A., Tang, Y.S., Zijlmans, R., Braban, C.F., Niederhauser, B., 2022. Intercomparison of in situ measurements of ambient NH_3: instrument performance and application under field conditions. Atmospheric Meas. Tech. 15, 6755–6787. http://dx.doi.org/10.5194/amt-15-6755-2022.

Van Damme, M., Clarisse, L., Franco, B., Sutton, M.A., Erisman, J.W., Kruit, R.W., Van Zanten, M., Whitburn, S., Hadji-Lazaro, J., Hurtmans, D., 2021. Global, regional and national trends of atmospheric ammonia derived from a decadal satellite record. Environ. Res. Lett. 16, 55017. http://dx.doi.org/10.1088/1748-9326/abd5e0.

Van Damme, M., Wichink Kruit, R.J., Schaap, M., Clarisse, L., Clerbaux, C., Coheur, P.F., Dammers, E., Dolman, A.J., Erisman, J.W., 2014. Evaluating 4 years of atmospheric ammonia (NH_3) over europe using IASI satellite observations and LOTOS-EUROS model results. J. Geophys. Res. - Atmospheres 119, 9549–9566. http://dx.doi.org/10.1002/2014JD021911.

Viana, M., Chi, X., Maenhaut, W., Querol, X., Alastuey, A., Mikuska, P., Vecera, Z., 2006. Organic and elemental carbon concentrations in carbonaceous aerosols during summer and winter sampling campaigns in Barcelona, Spain. Atmos. Environ. 40, 2180–2193. http://dx.doi.org/10.1016/j.atmosenv.2005.12.001.

Viana, M., Reche, C., Amato, F., Alastuey, A., Querol, X., Moreno, T., Lucarelli, F., Nava, S., Calzolai, G., Chiari, M., Rico, M., 2013. Evidence of biomass burning aerosols in the Barcelona urban environment during winter time. Atmos. Environ. 72, 81–88. http://dx.doi.org/10.1016/j.atmosenv.2013.02.031.

WHO, 2021. Who global air quality guidelines. In: Particulate Matter ($PM_{2.5}$ and PM_{10}), Ozone, Nitrogen Dioxide, Sulfur Dioxide and Carbon Monoxide. World Health Organization, Geneva, p. 290.

WHO, 2025. Agriculture – Sectoral Solutions for Air Pollution and Health: Technical Brief. World Health Organization, Geneva, http://dx.doi.org/10.2471/B09401, WHO Air Quality, Energy and Health Science and Policy Summaries.

Wing, S., Wolf, S., 2000. Intensive livestock operationsm, health, and quality of life among Eastern North Carolina residents. Environ. Health Perspect. 108 (3), 233–238. http://dx.doi.org/10.2307/3454439.

Wyer, K.E., Kelleghan, D.B., Blanes-Vidal, V., Schauberger, G., Curran, T.P., 2022. Ammonia emissions from agriculture and their contribution to fine particulate matter: a review of implications for human health. J. Environ. Manag. 323, 116285. http://dx.doi.org/10.1016/j.jenvman.2022.116285.